Combination of a reaction cell and an ultra-high vacuum system for the in situ preparation and characterization of a model catalyst

Yi-Jing Zang,[1,4#] Shu-Cheng Shi,[2#] Yong Han,[2,3*] Hui Zhang,[1] Wei-Jia Wang,[2] Peng Liu,[3] Mao Ye,[1] and Zhi Liu[1,2,3*]

[1] State Key Laboratory of Functional Materials for Informatics, Shanghai Institute of Microsystem and Information Technology, Chinese Academy of Sciences, Shanghai 200050, China.

[2]School of Physical Science and Technology, ShanghaiTech University, Shanghai 201210, China.

[3]Center for Transformative Science, ShanghaiTech University, Shanghai 201210, China.

[4]University of Chinese Academy of Sciences, Beijing 100049, China.

[#]These authors contributed equally.

[*]Corresponding author: hanyong@shanghaitech.edu.cn, liuzhi@shanghaitech.edu.cn

chinaXiv:202306.00010v1

Abstract: An in-depth understanding of the structure-activity relationship between the surface structure, chemical composition, adsorption and desorption of molecules, and their reaction activity and selectivity is necessary for the rational design of high-performance catalysts. Herein, we present a method for studying catalytic mechanisms using a combination of in situ reaction cells and surface science techniques. The proposed system consists of four parts: preparation chamber, temperature-programmed desorption (TPD) chamber, quick load-lock chamber, and in situ reaction cell. The preparation chamber was equipped with setups based on the surface science techniques used for standard sample preparation and characterization, including an Ar^+ sputter gun, Auger electron spectrometer, and a low-energy electron diffractometer. After a well-defined model catalyst was prepared, the sample was transferred to a TPD chamber to investigate the adsorption and desorption of the probe molecule, or to the reaction cell, to measure the catalytic activity. A thermal desorption experiment for methanol on a clean Cu(111) surface was conducted to demonstrate the functionality of the preparation and TPD chambers. Moreover, the repeatability of the in situ reaction cell experiment was verified by CO_2 hydrogenation on the Ni(110) surface. At a reaction pressure of 800 Torr at 673 K, turnover frequencies for the methanation reaction and reverse water-gas shift (RWGS) reaction were 0.15 and 7.55 Ni atom^{-1}s^{-1}, respectively.

Key words: Surface science; Model catalysts; Ultra-high vacuum; Temperature-programmed desorption; In situ reaction cell

chinaXiv:202306.00010v1

Introduction

Heterogeneous catalysis plays a crucial role in human life, and is involved in approximately 90% of the chemical processes.[1] Currently, chemical production accounts for approximately 25% of the energy used worldwide, which is expected to increase to 40% by 2040.[2] However, the excessive consumption of fossil fuels has led to an increase in global surface temperatures by 1.1 ℃ compared to the pre-industrial era, thereby posing a significant threat to both the environment and climate.[3] The need for the sustainable development of human society through net zero CO_2 emissions along with substantial reductions in other greenhouse gas emissions in the future has been widely recognized.[4-7] To achieve this goal, an atomic-scale understanding of the reaction mechanisms is required to develop efficient catalysts to maximize the utilization of energy.[2, 8-10]

Heterogeneous catalysis is an extremely complex process that involves multiple factors,[1-2] such as the space, time, pressure, and temperature. Industrial catalysts are considerably complex; for example, they are composed of catalysts, promoters, and supports with various surface structures and morphologies. Hence, researchers previously mainly used the traditional “trial-and-error” approach to develop high-performance catalysts and optimize reaction conditions.[2] Owing to the advantage of ultra-high vacuum (UHV) techniques and the subsequent development of surface science methods in the 1960s, the clean surfaces of single crystals (model catalysts) were used to study the surface properties at the atomic level for the first time.[9, 11] Over the past few decades, numerous surface science techniques have been developed to study surface properties.[9] Generally, these surface science techniques mainly include electron and ion spectroscopy, scanning probe microscopy, vibrational spectroscopy, diffraction techniques, and mass spectrometry.[9, 12]

Benefitting from the new techniques and instrumentation, surface science technology enables the study of catalysis on the atomic scale, and the discipline has emerged as a frontier area in physical chemistry.[9, 13-16] The surface science approach along with the reaction cell system can provide information regarding the surface structure and chemical composition in addition to the kinetic data of a reaction.[12, 17-18] Professors Ertl and Somorjai pioneered the study of the catalytic reaction mechanisms based on surface science and demonstrated significant achievements over the past 50 years.[9, 19-21] Currently, the fundamental study of reaction mechanisms based on model catalysts remains a widely used technique that plays an important role in the field of electrocatalysis.[22-24] Herein,

we present a study regarding the fundamental catalytic mechanisms using a setup that is a combination of a reaction cell and UHV system. The accessible pressure range of this system is 10^{-10} – 10000 mbar. Moreover, a standard flag-type sample holder was used. Using a vacuum suitcase, the sample can be transferred to other characterization systems without exposure to the atmosphere. Using the developed system, a model catalyst was prepared and its surface properties, such as the chemical composition, adsorption, and desorption of molecules, were characterized. Based on the in situ reaction cell measurements obtained, we expect to achieve an atomic-scale understanding of the structure-activity relationship between the surface properties and catalytic activity.

Experimental Section

A. System overview

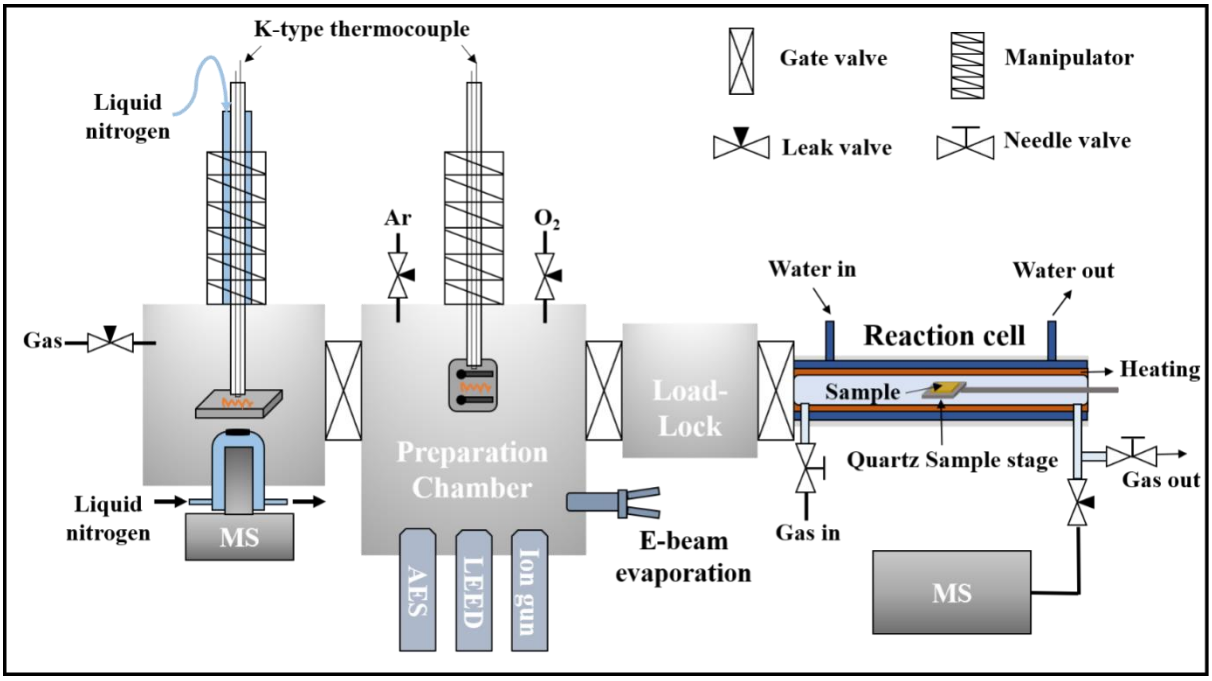

Fig. 1. Schematic of the overall system consisting of the UHV chambers and in situ reaction cell.

The system consists of four main parts. **Fig. 1** presents a schematic of the combination of a UHV system and an in situ reaction cell; the temperature-programmed desorption (TPD) chamber, preparation chamber, quick load-lock chamber, and in situ reaction cell are demonstrated (left to right). The system was designed with the help of (FERMION Instruments (Shanghai) Co., Ltd.), by which the chambers, manipulators, reaction cells, and supports were manufactured. The specimen was

chinaXiv:202306.00010v1

mounted on a flag-type sample holder and the temperature was measured using a K-type thermocouple. The sample stage in the load-lock chamber can store six samples simultaneously. As shown in **Fig. 1**, the load-lock chamber is connected to the preparation chamber and in situ reaction cell. In the preparation chamber, clean surfaces were obtained using standard sputtering and annealing cycles. The surface structure and cleanliness were verified using low-energy electron diffraction (LEED) and Auger electron spectroscopy (AES), respectively.

The preparation chamber has more than three ports for the installation of evaporation sources that can be used to grow thin films and deposit metal nanoparticles. After a model catalyst was prepared and characterized in the preparation chamber, it was transferred either to the TPD chamber for the thermal desorption experiment of the probe molecule or to the in situ cell through the load-lock chamber for activity measurements. Herein, detailed descriptions of the components and parameters of the preparation chamber, TPD chamber, and in situ reaction cell are provided.

B. Preparation chamber

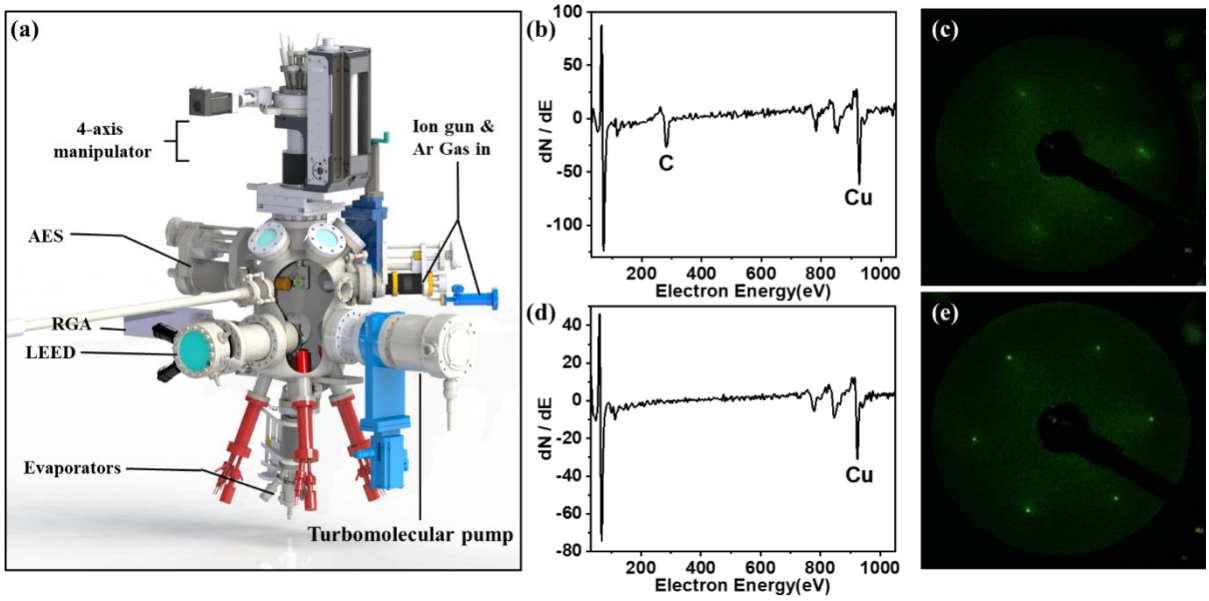

Fig. 2. (a) Schematic of the preparation chamber. (b) AES spectrum and (c) LEED pattern (electron energy, 100 eV) of the Cu(111) surface without cleaning treatment. (d) AES spectrum and (e) LEED pattern (electron energy, 100 eV) of the clean Cu(111) surface.

The preparation chamber (**Fig. 2a**) was a stainless-steel cylinder equipped with a four-axis manipulator system consisting of a manipulator, an XYZ stage (X, Y transfer distance, 25 mm; Z transfer distance, 210 mm), and a differentially pumped rotary platform (DN 100CF, 360° rotatable).

chinaXiv:202306.00010v1

A turbomolecular pump (STP-301, EDWARDS) and turbomolecular pumping station (nEXT 85D-CF63/nXDS6i, EDWARDS) were used collaboratively in the pump chamber. The pressure of the preparation chamber was measured using an ion gauge (UHV-24, Agilent); the base pressure was 2×10^{-10} Torr.

Flag-type sample holders can be composed of different materials such as stainless steel, tantalum, and molybdenum. Unless stated otherwise, an Inconel sample holder was used. The sample was annealed via electron beam heating within a temperature range between 300–1500 K. A K-type thermocouple that was closer to the sample was spot-welded at the end of the manipulator. The temperature difference between the thermocouple and the sample surface was calibrated through direct measurements using a pyrometer (IGA 8 pro, IMPAC). The preparation chamber was equipped with an ion source (IS 40C1 ION SOURCE, PREVAC), AES (microCMA, RBD), and LEED (BDL600IP-3GR, OCI). A Cu(111) single crystal (diameter of 10 mm; thickness of 2 mm) was purchased from MaTecK GmbH (Germany). As shown in **Fig. 2b**, C was the main contaminant on the uncleaned Cu (111) surface, resulting in a blurry p(1 × 1) LEED pattern (**Fig. 2c**). After several cycles of Ar^+ sputtering (1.5 keV, 15 min) and annealing at 810 K for 10 min,[25] a clean Cu(111) surface was obtained (**Fig. 2d**). The sharp p(1 × 1) diffraction pattern (**Fig. 2e**) further confirms that the clean Cu(111) surface was well prepared.

C. TPD chamber

The TPD chamber (**Fig. 3a**) was a stainless-steel truncated cube equipped with a four-axis manipulator system consisting of a manipulator, XYZ stage (X, Y transfer distance of 25 mm; Z transfer distance of 150 mm), and a differentially pumped rotary platform (DN 100CF, 360° rotatable). The chamber was pumped using a combination of a turbomolecular pump (STP-301, EDWARDS) and turbomolecular pumping station (nEXT 85D-CF63/nXDS6i, EDWARDS) shared with the preparation chamber. The pressure of the TPD chamber was measured using an ion gauge (UHV-24, Agilent), and the base pressure was 1×10^{-10} Torr.

To accurately measure the sample temperature, a K-type thermocouple was placed in direct contact with the sample. The sample was annealed using either hot filament radiation or electron-beam heating and cooled by adding liquid nitrogen to the cold trap of the manipulator (**Fig. 3a**). The

chinaXiv:202306.00010v1

sample temperature was varied from 80–1000 K and increased linearly from 100–600 K through proportional-integration-differentiation (PID) heating power control. **Fig. 3b** presents the sample temperature (black line) and setpoint (red line) during the linear heating process at a rate of 1 K/s, indicating excellent linearity of the heating curve.

The probe molecule was exposed to the sample surface by backfilling, or through a leak valve (ZLVM94R, Vacgen). A stainless-steel doser (inner diameter of 5 mm) was mounted on the TPD chamber using a linear shift (**Fig. 3a**), which could be moved to a position in front of the sample surface. During the TPD experiment, the distance between the sample surface and the collecting hole (5 mm in diameter) on the shield of the quadrupole mass spectroscopy (QMS) instrument (RC PIC Analyzer, HIDEN) was approximately 2 mm. Moreover, the shield was cooled by a liquid nitrogen flow, which acted as a differential pumping system.

chinaXiv:202306.00010v1

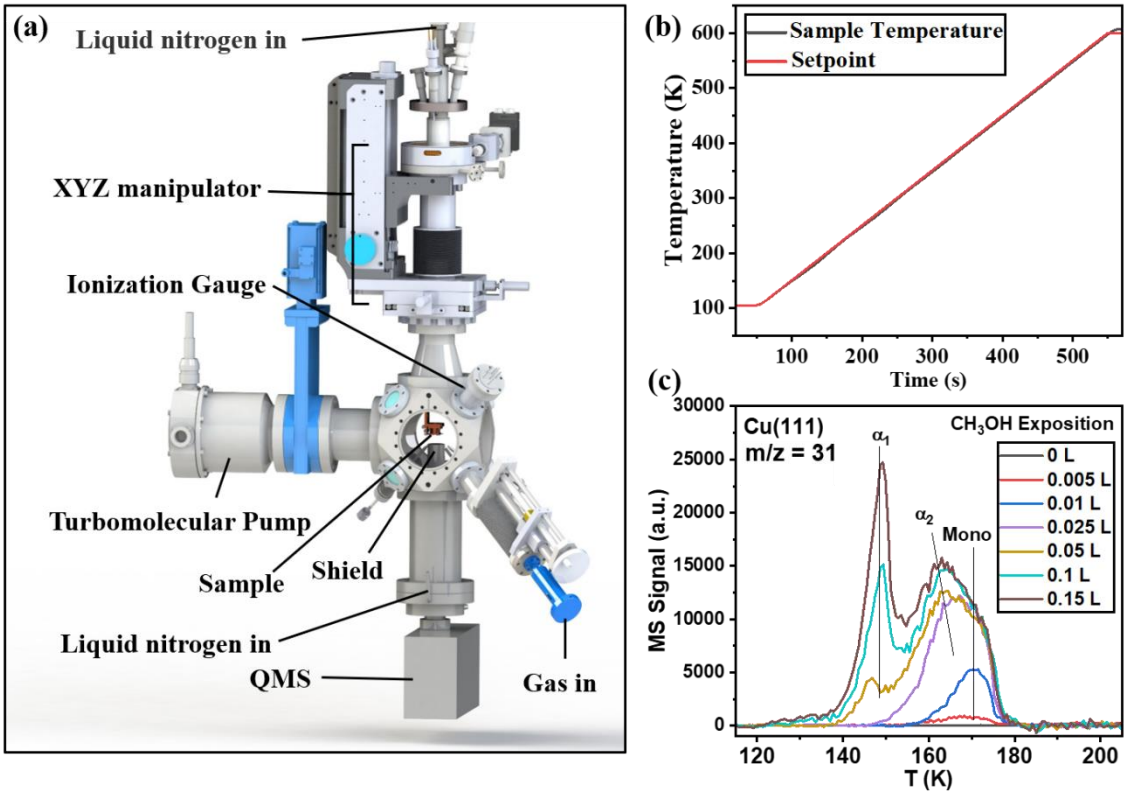

Fig. 3. (a) Schematic of the TPD chamber. (b) Temperature-programmed curve ranging from 100 to 600 K with a rate of 1 K/s; the black and red lines indicate the sample temperature and the setting point, respectively. (c) TPD spectra obtained with different doses (0, 0.005, 0.01, 0.025, 0.05, 0.1, and 0.15 L, respectively) of methanol on the Cu(111) surface.

D. In situ reaction cell

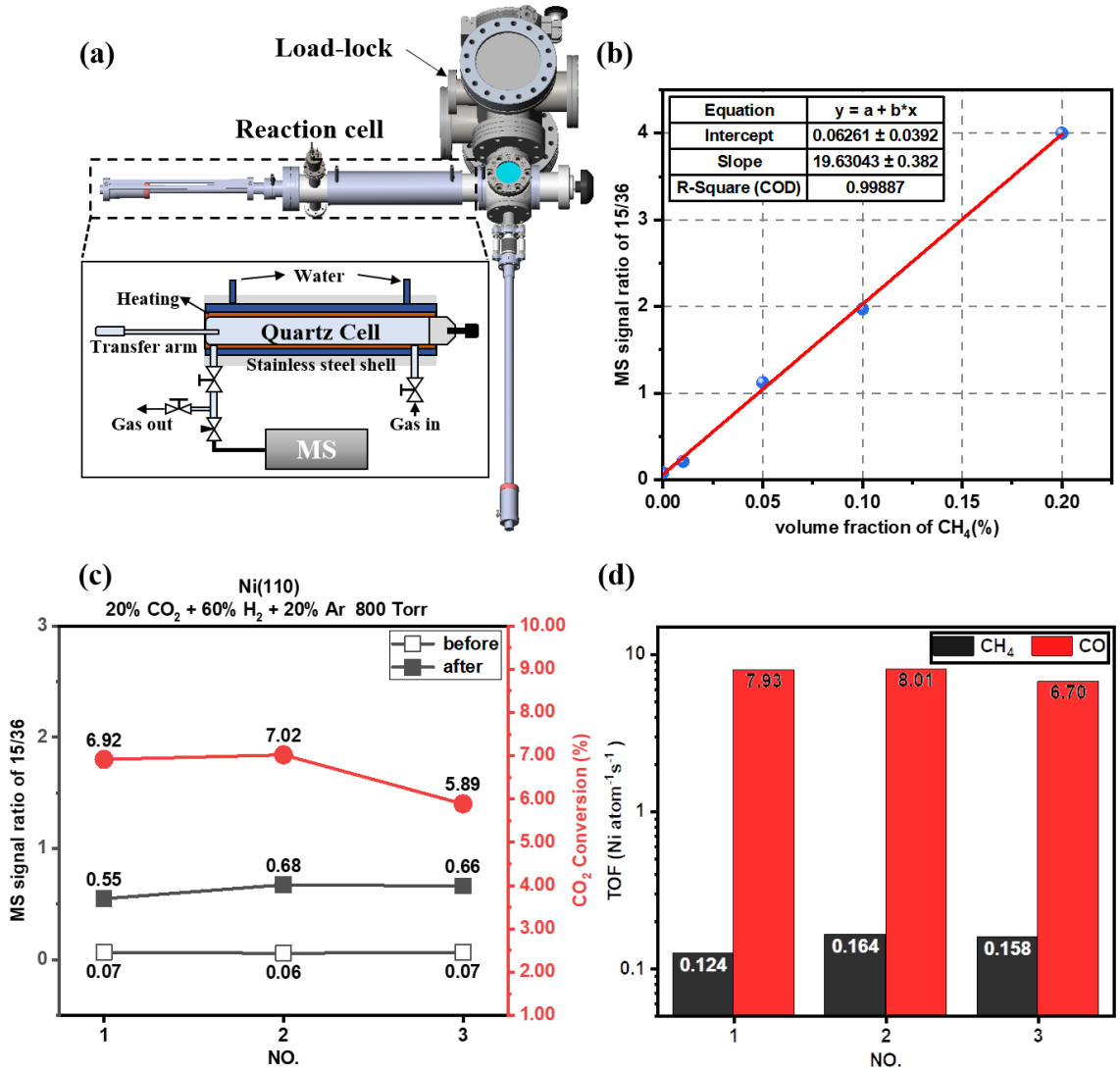

Fig. 4. (a) Schematic of the load-lock chamber and in situ reaction cell. (b) Working curve of the volume fraction of CH_4 versus the MS signal ratio of 15/36. (c) MS signal ratio of 15/36 before and after the reaction as well as the CO_2 conversion on the Ni(110) surface. Reaction conditions: 800 Torr gas mixture (20% CO_2, 60% H_2, and 20% Ar), 673 K, 3600 s. (d) TOFs of the methanation reaction and RWGS reaction on the Ni(110) surface.

The in situ reaction cell was connected to a load-lock chamber (**Fig. 4a**). The prepared samples were transferred to a reaction cell to measure their catalytic activity without atmospheric exposure. As shown in the inset of **Fig. 4a**, the main part of the reaction cell consisted of a quartz cell and a stainless-steel shell. The volume of the quartz cell was 93 cm^3, and it was heated using a resistance wire, which was controlled using a PID setting. The temperature ranged between 300–1200 K, and a K-type thermocouple was used to measure the reaction temperature. To minimize the background reaction,

chinaXiv:202306.00010v1

the sample stage of the reaction cell was composed of quartz. The base pressure of the reaction cell was reduced to less than 5×10^{-8} Torr, while the working pressure limit was 10 bar. The flows at the inlet and outlet of the reaction gas chamber were controlled using two needle valves (inset of **Fig. 4a**). The reaction pressure was measured using a Baratron capacitance gauge (range: 1–1000 Torr, 626D, MKS). To minimize the effect of the dead volume, we placed the two needle valves as close as possible to the reaction cell. Hence, the dead volume was approximately 4 cm^3. Considering that the volume of the reactor was 93 cm^3, the effect of the dead volume can be neglected. The reaction products were analyzed using QMS (RC PIC Analyzer, HIDEN). The base pressure of MS was 1×10^{-10} Torr.

The operating conditions of the reaction cell can be static (batch reactor) or dynamic (flow cell), depending on the reaction rate. The former favors the accumulation of products and is suitable for reactions with low turnover frequencies (TOFs). There is a heat insulation layer between the heating wire and stainless-steel shell. During the experiments, this part was maintained under vacuum to protect the heating filament. In the next section, we present the CO_2 hydrogenation reaction on the Ni(110) surface as an example to illustrate the performance of the in situ reaction cell (**Fig. 4b-d**).

chinaXiv:202306.00010v1

Results and Discussion

A. Testing the TPD system

TPD of methanol on the clean Cu(111) surface: The thermal desorption of methanol from a clean Cu(111) surface was performed after exposure to methanol at 90 K. Before the experiments, methanol (99.9%, Macklin) was purified by conducting several freeze-pump-thaw cycles, and the dosing gas line for methanol was baked under vacuum conditions ($<10^{-6}$ Torr) and then flushed several times with high-purity methanol vapor. Approximately 45 min were required to cool the sample from room temperature (RT) to 90 K for the first time. Subsequently, the sample was flushed at 600 K to remove any residual gas adsorbed on the clean surface from the chambers during the cooling process. Thereafter, the sample was cooled once again to 90 K within 15 min because the sample stage was cooled with liquid nitrogen.

At 90 K, the pressure of methanol during adsorption ranged between 5×10^{-10} and 2×10^{-9} Torr, and the doser was moved to approximately 50 mm in front of the Cu(111) surface. **Fig. 3c** presents the TPD spectra for methanol on the Cu(111) surface at doses of 0, 0.005, 0.01, 0.025, 0.05, 0.1, and 0.15

L (1.33 L = 1 × 10^{-6} Torr·s). The heating rate was 1 K/s and the MS signal of methanol was measured at m/z = 31. At significantly small dosages (0.005 and 0.01 L), only one desorption peak was observed at approximately 170 K (**Fig. 3c**), which was assigned to the desorption of the methanol monolayer on the Cu(111) surface.[26] At a dosage higher than 0.01 L, two new desorption peaks (α_1 and α_2) appeared at approximately 149 K and 162 K (**Fig. 3c**), respectively. These two peaks originated from the desorption of the methanol multilayers and the amorphous second layer.[26-29]

B. Testing the in situ reaction cell

Measurement of the activity for CO_2 hydrogenation on the Ni(110) surface: Ni is among the most important non-precious metal catalysts for CO_2 hydrogenation.[30-31] An atomic-scale understanding of the reaction mechanism is essential for the rational design of high-performance catalysts. In this study, an in situ reaction cell was used to measure the TOFs of methanation and the reverse water-gas shift (RWGS) reaction on the Ni(110) surface during CO_2 hydrogenation (**Fig. 4b-d**).

Before the activity measurement on the Ni(110) surface, only the sample holder (without the sample) was transferred to the in situ reaction cell for the blank experiment. The reactant was a mixture of 20% CO_2, 60% H_2, and 20% Ar, with Ar used as the internal standard. The conversion of CO_2 was obtained by measuring the MS signal of CO_2 (m/z = 44), which was calibrated using Ar (m/z = 40) before and after the reaction at a working pressure of 2 × 10^{-8} Torr. To quantify the methane in the products, we constructed a working curve (**Fig. 4b**) of the methane fraction versus an MS signal ratio of 15/36 from the calibration gases (working pressure 1 × 10^{-6} Torr), which were prepared by adding 0.01%, 0.05%, 0.1% and 0.2% methane to the reactants. Because the methane content in the product was significantly low, we used the more sensitive fragment signal (36) of Ar for calibration. In the blank experiment, the CO_2 conversion was less than 1%, and the MS signal ratio of 15/36 did not change under the set reaction conditions (800 Torr, 673 K, 3600 s) (**Fig. 4c**), indicating that the background reaction was negligible.

A Ni(110) single crystal (10 mm × 10 mm and 1 mm thickness) was purchased from Hefei Ke Jing Materials Technology Co., Ltd., China. The backside of the single crystal was passivated with a 50 nm SiO_2 film. After Ar^+ sputtering (1.5 keV, 10 min) and annealing (900 K, 10 min), clean Ni(110) was transferred to the in situ reaction cell without exposure to the atmosphere. As shown in Fig. 5, the

chinaXiv:202306.00010v1

AES and LEED patterns demonstrated that Ni(110) retained its single-crystal structure after the reaction. The activity for CO_2 hydrogenation on the Ni(110) surface was measured three times. As shown in **Fig. 4c**, the CO_2 conversion was maintained within approximately 6% at 800 Torr and 673 K within a reaction time of 3600 s. Considering the MS signal ratio of 15/36 for the product (**Fig. 4c**) and the working curve (**Fig. 4c**), the fraction of methane in the product was determined. The reaction surface area of Ni(110) was 1 cm^2, and the number of Ni atoms per unit area on the Ni(110) surface was 1.14×10^{15}.[32] As the amount of carbon did not change before and after the reaction, we calculated the fraction of CO from the carbon balance. According to the aforementioned results, TOFs of the methanation and RWGS reactions on the Ni(110) surface were 0.15 ± 0.03 and 7.55 ± 0.85 Ni $atom^{-1}s^{-1}$, respectively **(Fig. 4d)**. Using silica-supported Ni nanoclusters with well-controlled average-sized particles, Vogt et al. demonstrated that the TOFs of the methanation reaction ranged between 0.016–0.05 per surface Ni atom per second.[31] We observed that the TOFs of the methanation reaction on the Ni(110) surface were higher than those on silica-supported Ni catalysts, which is consistent with the theoretical prediction of the methanation reaction activity on the Ni surfaces following the order of 110 > 211 > 111 > 100.[33-34]

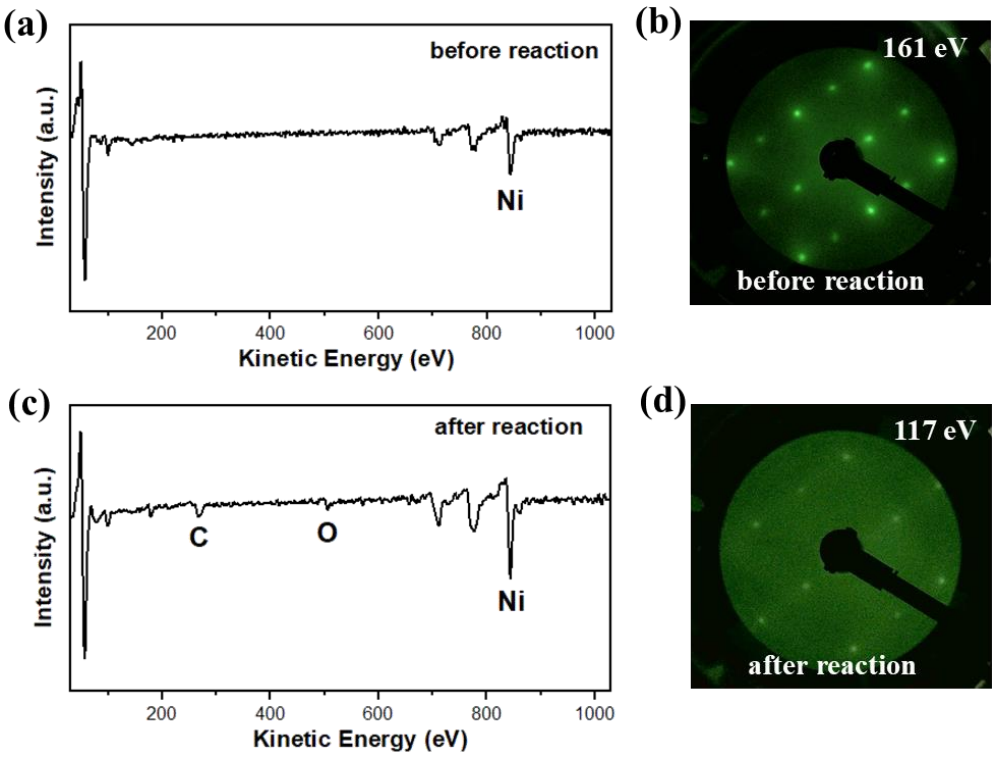

Fig. 5. AES spectra of the Ni(110) surface (a) before and (c) after the reaction, and LEED patterns of the Ni(110) surface (b) before and (d) after the reaction.

chinaXiv:202306.00010v1

Conclusions

To study the structure-activity relationship between the surface properties and catalytic performance, we combined the surface techniques and in situ reaction cells into a single system. This apparatus consisted of a preparation chamber, a TPD chamber, a load-lock chamber, and an in situ reaction cell. The base pressures of the preparation and TPD chambers were better than 2×10^{-10} Torr. In the preparation chamber, we performed standard sputtering and annealing (300–1500 K) treatments on the sample to obtain a clean surface and physical vapor deposition to grow thin films and nanoclusters. Subsequently, LEED and AES were used to determine the surface structures and components, respectively. The thermal desorption experiment of a probe molecule on a well-defined surface was performed in a TPD chamber within temperatures ranging between 100–600 K. Benefitting from the use of this system, the well-prepared sample can be transferred to an in situ reaction cell for the measurement of catalytic activity within 300–1200 K at pressures up to 10 bar without exposure to the atmosphere. We expect that this system will become a powerful tool for studying catalytic mechanisms in the near future.

chinaXiv:202306.00010v1

Acknowledgements

This work was supported by the National Natural Science Foundation of China (Grant Nos. 21802096, 21832004, 21902179, 21991152, and 21991150) and the Shanghai XFEL Beamline Project (SBP) (3101150550588592016 1A2101001). H.Z. acknowledges the support of the Shanghai Sailing Program (19YF1455600).

References

1. M. Boudart, B. H. Davis, H. Heinemann, Introduction, in *Handbook of Heterogeneous Catalysis*. ed. by G. Ertl, H. Knözinger, J. Weitkamp (John Wiley & Sons, 1997), p.1-48 https://doi.org/10.1002/9783527619474.ch1
2. C. Reece, R. J. Madix, Moving from fundamental knowledge of kinetics and mechanisms on surfaces to prediction of catalyst performance in reactors. ACS Catal. **11**, 3048-3066 (2021). https://doi.org/10.1021/acscatal.0c05173
3. IEA (2021), World Energy Outlook 2021, IEA, Paris https://www.IEA.org/Reports/World-

Energy-Outlook-2021.
4. D. Wang, Z. Xie, M. D. Porosoff, J. G. Chen, Recent advances in carbon dioxide hydrogenation to produce olefins and aromatics. Chem. **7**, 2277-2311 (2021). https://doi.org/10.1016/j.chempr.2021.02.024
5. X. Jiang, X. Nie, X. Guo, C. Song, J. G. Chen, Recent advances in carbon dioxide hydrogenation to methanol via heterogeneous catalysis. Chem. Rev. **120**, 7984-8034 (2020). https://doi.org/10.1021/acs.chemrev.9b00723
6. M. Wang, L. Luo, C. Wang, J. Du, H. Li, J. Zeng, Heterogeneous catalysts toward CO_2 hydrogenation for sustainable carbon cycle. Acc. Mater. Res. **3**, 565-571 (2022). https://doi.org/10.1021/accountsmr.2c00006
7. J. Low, J. Ma, J. Wan, W. Jiang, Y. Xiong, Identification and design of active sites on photocatalysts for the direct artificial carbon cycle. Acc. Mater. Res. **3**, 331-342 (2022). https://doi.org/10.1021/accountsmr.1c00222
8. D. Gao, R. M. Arán-Ais, H. S. Jeon, B. Roldan Cuenya, Rational catalyst and electrolyte design for CO_2 electroreduction towards multicarbon products. Nat. Catal. **2**, 198-210 (2019). https://doi.org/10.1038/s41929-019-0235-5
9. G. A. Somorjai, Y. Li, Introduction to surface chemistry and catalysis. 2 nd Edition. (John Wiley & Sons, 2010). ISBN: 978-0-470-50823-7
10. Y. Liu, D. Deng, X. Bao, Catalysis for selected C1 chemistry. Chem. **6**, 2497-2514 (2020). https://doi.org/10.1016/j.chempr.2020.08.026
11. G. Ertl, Reactions at surfaces: from atoms to complexity (Nobel Lecture). Angew. Chem. Int. Ed. **47**, 3524-35 (2008). https://doi.org/10.1002/anie.200800480
12. F. Morfin, L. Piccolo, A versatile elevated-pressure reactor combined with an ultrahigh vacuum surface setup for efficient testing of model and powder catalysts under clean gas-phase conditions. Rev. Sci. Instrum. **84**, 094101 (2013). https://doi.org/10.1063/1.4818669
13. J. Cai, Q. Dong, Y. Han, B.-H. Mao, H. Zhang, P. G. Karlsson, J. Åhlund, R.-Z. Tai, Y. Yu, Z. Liu, An APXPS endstation for gas–solid and liquid–solid interface studies at SSRF. Nucl. Sci. Tech. **30**, 81 (2019). https://doi.org/10.1007/s41365-019-0608-0
14. R. Chang, R.-Z. Tai, D. E. Starr, H. Bluhm, Z. Liu, Synchrotron radiation-based ambient pressure photoelectron spectroscopy and its applications. Nucl. Tech. **35**, 481-485 (2012).
15. H. Wu, Y. Yang, P. H. L. Jerry, Z. Liu, Y. Luo, M. Fan, A novel apparatus for operando rapid characterization on real reaction: design and application. Nucl. Tech. **39**, 100101, (2016). https://doi.org/10.11889/j.0253-3219.2016.hjs.39.100101.
16. L. Mayr, R. Rameshan, B. Klotzer, S. Penner, C. Rameshan, Combined UHV/high-pressure catalysis setup for depth-resolved near-surface spectroscopic characterization and catalytic testing of model catalysts. Rev. Sci. Instrum. **85**, 055104 (2014). https://doi.org/10.1063/1.4874002
17. A. L. Cabrera, N. D. Spencer, E. Kozak, P. W. Davies, G. A. Somorjai, Improved instrumentation to carry out surface analysis and to monitor chemical surface reactions in situ on small area catalysts over a wide pressure range (10^{-8} - 10^{5} Torr). Rev. Sci. Instrum. **53**, 1888-1893 (1982). https://doi.org/10.1063/1.1136899
18. J. Rodriguez, D. W. Goodman, High-pressure catalytic reactions over single-crystal metal surfaces. Surf. Sci. Rep. **14**, 1-107 (1991). https://doi.org/10.1016/0167-5729(91)90002-F
19. R. Imbihl, G. Ertl, Oscillatory kinetics in heterogeneous catalysis. Chem. Rev. **95**, 697-733 (1995). https://doi.org/10.1021/cr00035a012

chinaXiv:202306.00010v1

chinaXiv:202306.00010v1

20. J. Y. Park, L. R. Baker, G. A. Somorjai, Role of hot electrons and metal–oxide interfaces in surface chemistry and catalytic reactions. Chem. Rev. **115**, 2781-2817 (2015). https://doi.org/10.1021/cr400311p
21. G. A. Somorjai, R. L. York, D. Butcher, J. Y. Park, The evolution of model catalytic systems; studies of structure, bonding and dynamics from single crystal metal surfaces to nanoparticles, and from low pressure ($<10^{-3}$ Torr) to high pressure ($>10^{-3}$ Torr) to liquid interfaces. Phys. Chem. Chem. Phys. **9**, 3500-13 (2007). https://doi.org/10.1039/b618805b
22. F. Faisal, M. Bertram, C. Stumm, F. Waidhas, O. Brummel, J. Libuda, Preparation of complex model electrocatalysts in ultra-high vacuum and transfer into the electrolyte for electrochemical IR spectroscopy and other techniques. Rev. Sci. Instrum. **89**, 114101 (2018). https://doi.org/10.1063/1.5047056
23. F. Faisal, C. Stumm, M. Bertram et al., Electrifying model catalysts for understanding electrocatalytic reactions in liquid electrolytes. Nat. Mater. **17**, 592-598 (2018). https://doi.org/10.1038/s41563-018-0088-3
24. C. Li, J. Cai, T. Yang, Y. Han, Q. Dong, Y. Li, Z. Liu, In-situ studies of CO oxidation on Pt(110). Nucl. Tech. **41**, 120501 (2018). https://doi.org/10.11889/j.0253-3219.2018.hjs.41.120501
25. T. Yang, T. Gu, Y. Han et al., Surface orientation and pressure dependence of CO_2 activation on Cu surfaces. J. Phys. Chem. C **124**, 27511-27518 (2020). https://doi.org/10.1021/acs.jpcc.0c08262
26. T. Koitaya, Y. Shiozawa, Y. Yoshikura, K. Mukai, S. Yoshimoto, J. Yoshinobu, Systematic study of adsorption and the reaction of methanol on three model catalysts: Cu(111), Zn–Cu(111), and oxidized Zn–Cu(111). J. Phys. Chem. C **121**, 25402-25410 (2017). https://doi.org/10.1021/acs.jpcc.7b09598
27. T. J. Lawton, J. Carrasco, A. E. Baber, A. Michaelides, E. C. H. Sykes, Hydrogen-bonded assembly of methanol on Cu(111). Phys. Chem. Chem. Phys. **14**, 11846-11852 (2012). https://doi.org/10.1039/C2CP41875D
28. R. B. David, A. B. Yaacov, B. Eren, Effect of surface orientation on methanol adsorption and thermally induced structural transformations on copper surfaces. J. Phys. Chem. C **125**, 6099-6107 (2021). https://doi.org/10.1021/acs.jpcc.0c10278
29. J. Gong, D. W. Flaherty, R. A. Ojifinni, J. M. White, C. B. Mullins, Surface chemistry of methanol on clean and atomic oxygen pre-covered Au(111). J. Phys. Chem. C **112**, 5501-5509 (2008). https://doi.org/10.1021/jp0763735
30. J. Cai, Y. Han, S. Chen, E. J. Crumlin, B. Yang, Y. Li, Z. Liu, CO_2 activation on Ni(111) and Ni(100) surfaces in the presence of H_2O: an ambient-pressure X-ray photoelectron spectroscopy study. J. Phys. Chem. C **123**, 12176-12182 (2019). https://doi.org/10.1021/acs.jpcc.8b11698
31. C. Vogt, E. Groeneveld, G. Kamsma, M. Nachtegaal, L. Lu, C. J. Kiely, P. H. Berben, F. Meirer, B. M. Weckhuysen, Unravelling structure sensitivity in CO_2 hydrogenation over nickel. Nat. Catal. **1**, 127-134 (2018). https://doi.org/10.1038/s41929-017-0016-y
32. K. Christmann, O. Schober, G. Ertl, Adsorption of CO on a Ni(111) surface. J. Chem. Phys. **60**, 4719-4724 (1974). https://doi.org/10.1063/1.1680972
33. C. Vogt, M. Monai, E.B. Sterk et al., Understanding carbon dioxide activation and carbon–carbon coupling over nickel. Nat. Commun. **10**, 5330 (2019). https://doi.org/10.1038/s41467-019-12858-3
34. E. B. Sterk, A. E. Nieuwelink, M. Monai, J. N. Louwen, E. T. C. Vogt, I. A. W. Filot, B. M. Weckhuysen, Structure sensitivity of CO_2 conversion over nickel metal nanoparticles explained by micro-kinetics simulations. JACS Au. **2**, 2714-2730 (2022). https://doi.org/10.1021/jacsau.2c00430

chinaXiv:202306.00010v1